LETTER • OPEN ACCESS

Historical transboundary ozone health impact linked to affluence

To cite this article: Lulu Chen *et al* 2022 *Environ. Res. Lett.* **17** 104014

View the article online for updates and enhancements.

ENVIRONMENTAL RESEARCH
LETTERS

LETTER

Historical transboundary ozone health impact linked to affluence

Lulu Chen[1,2], Jintai Lin[1,*], Ruijing Ni[1], Hao Kong[1], Mingxi Du[3], Yingying Yan[4], Mengyao Liu[5], Jingxu Wang[6], Hongjian Weng[1], Yuanhong Zhao[1], Chunjin Li[1] and Randall V Martin[2,7,8]

[1] Laboratory for Climate and Ocean-Atmosphere Studies, Department of Atmospheric and Oceanic Sciences, School of Physics, Peking University, Beijing 100871, People's Republic of China
[2] Department of Energy, Environmental and Chemical Engineering, Mckelvey School of Engineering, Washington University in St. Louis, St. Louis, MO 63130, United States of America
[3] School of Public Policy and Administration, Xi'an Jiaotong University, Xi'an 710049, China
[4] Department of Atmospheric Science and Technology, School of Environmental Sciences, China University of Geosciences, Wuhan 430074, People's Republic of China
[5] Royal Netherlands Meteorological Institute, De Bilt NL-3731, GA, The Netherlands
[6] Key Laboratory of Physical Oceanography, College of Oceanic and Atmospheric Sciences, Ocean University of China, Qingdao 266100, China
[7] Department of Physics and Atmospheric Science, Dalhousie University, Halifax NS B3H 4R2, Canada
[8] Smithsonian Astrophysical Observatory, Harvard-Smithsonian Center for Astrophysics, Cambridge, MA 02138, United States of America
* Author to whom any correspondence should be addressed.

E-mail: linjt@pku.edu.cn

Abstract

Ozone pollution is a major transboundary threat to global health. Systematic improvement of mitigation strategy for transboundary ozone requires a socioeconomic understanding of historical lessons in countries at different affluence levels. Here, we explore the changes in transboundary ozone related premature deaths over 1951–2019 driven by anthropogenic emissions of four country groups categorized by income level. By integrating global emission datasets, a chemical transport model (GEOS-Chem), *in situ* ozone measurements worldwide and an ozone exposure-response model, we find that mortality caused by transboundary anthropogenic ozone increases by 27 times from 1951 to 2019, and on average contributes about 27% of global anthropogenic ozone related deaths. All groups exert and suffer from substantial transboundary ozone related mortality. The high-income and upper middle groups have each experienced an inverted U-shaped relationship between its affluence and per-million-people contribution to mortality caused by transboundary ozone, with the turning point around 23 000 USD and 6300 USD, respectively. The lower middle group has gradually matched the growth pathway of the upper middle group with a turning point less clear. Concerted efforts to ensure early turning points in less affluent countries will have considerable global health benefits.

1. Introduction

Ozone in the surface air is estimated to cause hundreds of thousands of premature deaths each year through worsening respiratory and cardiovascular diseases [1–10]. Formed from emitted precursor gases such as nitrogen oxides (NO_x) and non-methane volatile organic compounds (NMVOCs) through highly nonlinear photochemistry, with a tropospheric lifetime of a few weeks, ozone can be transported long distances to other regions to exert transboundary impacts [11, 12]. Despite decades of mitigation efforts especially in developed regions, ozone remains a major transboundary pollutant [11–14]. Attempts to systematically improve strategies for transboundary ozone control in the future must learn from common lessons in the past. Historically, changes in regional anthropogenic emissions of ozone precursors are determined by energy consumption [15–17], energy structure [18], technology and emission control levels [19, 20], which are related to affluence level (indicated here

by per capita gross domestic product, GDP). Yet it remains unclear how regional affluence is linked to its contribution to mortality associated with transboundary ozone.

Previous works have attempted to link regional environmental issues to its affluence level, usually based on local empirical data [17, 21–24]. A few studies have connected regional affluence levels to their anthropogenic ozone-related emissions [17, 22–24]. However, emission-based assessments do not take into account the strong nonlinear ozone chemistry [25, 26]–with NMVOC emissions fixed, increasing NO_x emissions enhances ozone formation in the NO_x-limited chemical regime but decreases ozone in the NO_x-saturated regime [27]. Other studies have linked regional affluence level to its ambient ozone pollution [28–30], with an implicit assumption that ozone is fully derived from local precursor emissions. These studies do not isolate the impacts of transboundary ozone originating outside that region's territory. For example, Asia is an important source region of ozone over North America, and vice versus [11, 12, 14, 31, 32]. The long-distance transboundary ozone means that ozone concentrations worldwide contributed by a region's emissions (as a source) differ from ozone concentrations over that region's territory (as a receptor). In addition to the complex ozone chemistry [27] and transboundary transport [11, 12], the health response to ozone exposure may be nonlinear [3]. To date, a global-scale assessment of the potential connection between each region's transboundary ozone related health impact and its affluence level is lacking.

In this study, from a historical perspective, we quantify the impacts of regional anthropogenic emissions on global ozone-related premature mortality over 1951–2019, explore the role of transboundary pollution, and then reveal the linkage between regional transboundary impact and its affluence level. All countries are aggregated into four groups as emission source regions based on their per capita gross national income (GNI), as defined by the United Nations [33]. These groups include high-income (i.e. developed regions; with GNI per capita more than $12 235), upper middle income (e.g. China and Russia; with GNI per capita between $3956 and $12 235), lower middle income (e.g. India and Indonesia; with GNI per capita between $1006 and $3955) and low-income (GNI per capita less than $1005); see supplementary figure 1 of our previous study [34] for detailed regional disaggregation information. The classification of four groups is fixed, to explore the historical transboundary ozone related mortality impacts of country groups based on current worldwide economy. We only consider the impacts of emissions released in each group due to its production, and do not account for the emissions released in other groups associated with that group's consumption [35, 36].

2. Method and datasets

This section describes our methodology, datasets and uncertainty estimates. Briefly, our study integrates historical emission data from the Community Emissions Data System (CEDS) [37] and the Multiresolution Emission Inventory for China (MEIC) [20, 38–40], the chemical transport model GEOS-Chem [41], *in situ* ozone measurements worldwide and an ozone exposure-response model [3]. We estimate the transboundary ozone related mortality caused by anthropogenic emissions in each income group for about every five year. We fix the meteorological conditions of GEOS-Chem at the 2014 level to focus on the sole impacts of anthropogenic emissions (section 2.2); a sensitivity test shows that using year-specific meteorology has a small effect on ozone-related mortality results (supplementary figure 1). Simulated ozone concentrations by GEOS-Chem are evaluated and adjusted based on historical surface measurements (section 2.3). We employ Turner *et al* [3] ozone exposure-response model to estimate premature deaths of adults ($\geqslant$30 yr old) caused by respiratory and circulatory diseases associated with long-term exposure to ozone pollution. The model adopts a low concentration cutoff (LCC) of 26.7 ppbv as threshold below which ozone is assumed not to cause mortality [3]; choosing 0 ppbv as the LCC instead leads to a larger number of premature deaths and a strengthened relationship between regional affluence and its ozone morality impact (supplementary figure 2). Year-, country- and disease-specific baseline mortality rates since 1990 are calculated based on the Global Burden of Disease (GBD) 2019 database [42], and the rates at 1990 are applied to precious years [34]; a sensitivity test linearly extrapolating the rates to earlier years, following previous works [34, 43], shows slightly different mortality results (by 2%–23% depending on the years, supplementary figure 3).

2.1. Historical population and GDP data
The historical country-based GDP and population data are obtained from the World Bank [44] for 264 regions, covering the period from 1960 to 2019. The GDP data are expressed in constant 2010 USD. When we calculate per capita GDP of each income group, we do not consider a few small countries of which GDP data in earlier years are missing.

To extend per capita GDP data to 1951, we employ exponential linear extrapolation. For each income group, we calculate the growth rate of per capita GDP from 1960 to 1970 (equation (1)), and then extend the group-based per capita GDP to 1951 (equation (2))

$$\delta_i = \frac{\ln\left(G_p^{i,t2}\right) - \ln\left(G_p^{i,t1}\right)}{t2 - t1} \qquad (1)$$

$$\ln\left(G_p^{i,t}\right) = \delta_i * (t - t1) + \ln\left(G_p^{i,t1}\right). \qquad (2)$$

$G_p^{i,t}$ represents per capita GDP of country group i (high-income, upper middle income, lower middle income, or low-income) in the year t. The subscript p represents per capita. $t1$ denotes the year of 1960 and $t2$ the year of 1970. δ_i represents the growth rate of per capita GDP of group i.

2.2. GEOS-Chem model simulations

A global chemical transport model GEOS-Chem version 11-01 [41] is employed in this study, to estimate the global ozone concentrations about every five years, including 1951, 1955, 1960, 1965, 1970, 1975, 1980, 1985, 1990, 1995, 2000, 2005, 2010, 2014 and 2019. All simulations cover 18 months, with the first six months used for model spin-up (e.g. the simulation for 2014 covers July 2013 through December 2014). The model setup follows our previous study [34]. Briefly, all simulations are driven by the MERRA2 assimilated meteorology provided by the NASA Global Modeling and Assimilation Office. The meteorological data are fixed in 2014 to quantify the sole impact of anthropogenic emissions. Supplementary figure 1 shows the mortality results using year-specific meteorology for 1981, which are similar to those using 2014 meteorology. The model is run with the full O_x-NO_x-VOC-CO-HO_x gaseous chemistry, and aerosols are online calculated. The horizontal resolution is 2.5° longitude × 2° latitude grid with 47 vertical layers. Uptake of the hydroperoxyl radical (HO_2) on aerosols is accounted for with an uptake coefficient of 0.2, following previous works [14, 45]. Vertical mixing of planetary boundary layer follows Lin and McElroy [46] Model convection uses the relaxed Arakawa-Schubert scheme [47]. Stratospheric ozone follows the Linoz scheme [48].

We use monthly gridded (0.5° longitude × 0.5° latitude) CEDS data from Hoesly *et al* [37] for gaseous (NO_x, NMVOC, SO_2, NH_3) and primary aerosol (BC and POA) pollutants globally over 1951–2014. CEDS emissions over China are replaced by emissions from MEIC [20, 38–40] since the year of 2000, because CEDS does not well represent the changes in Chinese emissions. Then we employ the country- and species-specific temporal changes over 2015–2019 in emission data from McDuffie *et al* [49] to derive the emissions over 1951–2019. NMVOC and NO_x emissions of four groups are shown in supplementary figure 4. Supplementary material S1 and table S1 of our previous study [34] details more emission information, such as natural emission, international shipping and aviation emission inventories.

In each of the simulation years, we have six types of full-chemistry simulations to quantify surface ozone concentrations worldwide contributed by anthropogenic emissions of each country group. The control simulation (CTL) includes all anthropogenic emissions worldwide. Five sensitivity simulations zero out anthropogenic emissions worldwide and in four country groups group by group, including xANTH, xHIGH, xUPPER, xLOWER and xLOW. The difference between CTL and xHIGH represents the contribution of ozone by the high-income group, after the results are further adjusted to account for the nonlinear issue in ozone attribution (see below). The contributions of other groups are estimated in a similar way. International shipping emissions, aviation emissions and natural emissions are all included in xANTH simulations; we refer this part contribution as 'natural contribution'.

Considering the nonlinear relationship between ozone production and its precursors, we apply a linear weighted method to the model outputs on an hourly basis following a previous study [14]. For example, for the anthropogenic contribution of high-income group in each hour and grid cell, we first obtain the fraction of ozone contribution by this group to the total ozone summed based on the zero-out simulations:

$$f^{\text{HIGH}} = \frac{\text{CTL} - x\text{HIGH}}{[\text{CTL} - x\text{HIGH}] + [\text{CTL} - x\text{UPPER}] + [\text{CTL} - x\text{LOWER}] + [\text{CTL} - x\text{LOW}] + x\text{ANTH}}. \quad (3)$$

We then obtain the adjusted ozone contribution caused by the high-income group by applying f^{HIGH} to the total surface ozone in CTL:

$$\text{HIGH} = f^{\text{HIGH}} \times \text{CTL}. \quad (4)$$

Contributions of other groups are obtained similarly. The adjusted natural ozone is as follows:

$$\text{NATURE} = \frac{x\text{ANTH}}{[\text{CTL} - x\text{HIGH}] + [\text{CTL} - x\text{UPPER}] + [\text{CTL} - x\text{LOWER}] + [\text{CTL} - x\text{LOW}] + x\text{ANTH}} \times \text{CTL}. \quad (5)$$

2.3. GEOS-Chem evaluation and adjustment

We use ground-level ozone measurements worldwide to adjust for the effect of systematic model biases on our regional ozone attribution and health calculation. Hourly measurements in 2014 are taken from 1306 Environmental Protection Agency Air Quality System sites [50] for the US, from 216 sites of the National Air Pollution Surveillance program [51] for Canada, from 137 sites of European Monitoring and Evaluation Programme Chemical Coordination Centre network [52] for Europe, and from 945 sites of China National Environmental Monitoring Centre [53] for China. These data have been widely used for air quality assessment and other applications [54–56].

Since we use annual average daily maximum 8 h average (MDA8) ozone for health impact assessment (section 2.4), we further process the measurement data accordingly to facilitate comparisons with GEOS-Chem results. We convert the Chinese measurements from the original unit of μg m^{-3} at the standard condition (273.15 K and 1 atm) to mixing ratio (in ppbv). We further apply data quality control on all raw datasets, following a previous study [54]. We then convert the hourly data to MDA8, by calculating 8 h averages for 24 bins starting at 00:00 local time, and choose the highest of these 24 values. If there are less than six valid ozone values among each 8 h bin, the corresponding 8 h average value is considered missing. If there are two or more 8 h average values that are missing in a day, the corresponding MDA8 is considered missing. Lastly, we map all MDA8 data on a 2.5° longitude × 2.0° latitude grid for each day, with available data at all sites within a grid cell averaged to obtain the gridded MDA8 ozone.

We evaluate the annual average MDA8 ozone results of the CTL simulation. We first calculate the model MDA8 for each day and grid cell, and then select the model data only on days and in grid cells when the measured MDA8 data are available. As shown in the two columns on the left of supplementary figure 5, the CTL simulation overestimates the observed annual average MDA8 over China (by 9.8 ppbv on average), the US (by 8.9 ppbv), Europe (by 1.3 ppbv) and Canada (by 3.9 ppbv).

To remove the systematic model bias, we take a scaling approach in which a scaling factor (as the ratio of observed to CTL modeled annual mean MDA8 ozone) is derived for each range of population density (separated by yellow vertical lines in supplementary figure 6(a)). This population density-specific correction is used to facilitate the subsequent health impact calculations. It improves upon the approach by Shindell *et al* [2] that uses a single scaling factor for the whole globe. Here the scaling factors are derived as the average of the observed to modeled ratios in each population range, after combining all data in China, the US and Europe. Population data on a 0.1° × 0.1° grid are taken from GBD 2016 [57] health data and re-gridded to the model

resolution (2.5° longitude × 2.0° latitude). Generally, the (observed to modeled) ratios are less than 1 and tend to decrease with increasing population density. The scatter in the ratios reflects local characteristics not captured by the model simulation.

Although not used for scaling the model results, the ratios derived based on data in each region are shown separately in supplementary figures 6(b)–(d) for comparison. Both the US-based and China-based ratios (supplementary figures 6(b) and (c)) are close to the ratios based on all data in the US, China and Europe together (supplementary figure 6(a)), although the Europe-based ratios tend to be larger reflecting the smaller model biases over Europe.

We apply the three-country based ratios (supplementary figure 6(a)) to the whole globe. After scaling, the modeled population-weighted global annual average MDA8 ozone (37.6 ppbv) matches the observed value (37.9 ppbv) (supplementary table 1). Supplementary figure 5 (the two columns on the right) further shows that the scaling greatly reduces the model overestimation at individual grid cells. After scaling, the model bias is 1.3 ppbv averaged over China, 2.6 ppbv over the US, −4.2 ppbv over Europe, and −0.5 ppbv over Canada. The small bias for Canada indicates the robustness of our scaling approach, because the scaling factors are not derived based on Canadian measurements. To further test the robustness of our scaling approach over time, we employ the surface measurements over US and Europe in 2000. The results show our scaling approach effectively adjusts the modeled ozone to a small mean bias of 1.1 ppbv and −5.5 ppbv.

We then apply the scaling factors to all simulation years. For 1980 and earlier years when gridded GBD2016 population data are not available, we combine the gridded GBD2016 population data in 1990 with the historical country-based population time series from '*World Population Prospects*' [58].

We further quantify the capability of GEOS-Chem in simulating the historical background ozone concentrations. For this purpose, we employ long-term ozone measurements at 12 background sites from tropospheric ozone assessment report (TOAR) [59]. These sites are categorized as 'background' sites, have records before 1980 and have data for at least five years. Sites that are not included here do not satisfy both criteria. Supplementary table 2 shows the geographical information of these sites. For these 12 sites, maximum daily 8 h average data were averaged to obtain monthly mean values. When we calculate the annual means, the corresponding simulated monthly values are set as missing if the observed monthly ones are missing. Given the scarcity of historical measurement data, for each site we averaged all yearly mean measurement data within ten year of each simulation year (1951, 1960, 1970, 1980, etc) to match the respective model simulation. Model values are selected at the grid cell and height of each site. The scatter

plots in supplementary figure 7 show that GEOS-Chem reproduces the observed ozone both before and after the population-based adjustment, with a low bias and a slope close to 1 for each simulation year.

2.4. Premature mortality by ozone exposure

We use the pollution exposure-response relationship by Turner *et al* [3] to calculate the impact of annual average MDA8 ozone on premature mortality. This relationship is an update from Jerrett *et al* [60], and it has been widely used [1, 2, 5, 61]. For premature mortality caused by each of respiratory and circulatory (including diabetes) diseases:

$$M_g = b_g \times \left(1 - e^{-\beta \Delta O_g}\right) \times P_g \qquad (6)$$

$$\beta = \ln H / 10. \qquad (7)$$

Here, M_g represents the number of premature deaths caused by each disease due to exposure to annual average MDA8 ozone in grid cell *g*. The global total mortality is summed over all grid cells. b_g denotes the disease-specific gridded baseline mortality rate for people $\geqslant 30$ yr old, i.e. the fraction of total deaths caused by each disease. P_g denotes the number of people $\geqslant 30$ yr old exposed to ozone at grid cell *g*. The country-, year- and age-specific population data are from the '*World Population Prospects*' [58], and the gridded total population data are from GBD 2016 database [57]. The country-based age structure is applied to each grid cell within that country. The country-, disease-, age- and year-specific premature death data are from GBD 2019 data resources [42]. The baseline mortality rate of a country is calculated based on its population and mortality data, and is applied to all grid cells within that country. Since the GBD 2016 database provides mortality data since 1990, we apply the baseline mortality rates in 1990 to prior years.

β is the effect coefficient to present the association between annual average MDA8 ozone exposure and disease-specific premature mortality. It represents the natural logarithm of the Hazard Ratio (HR) for a 10 ppbv increase in ozone exposure. According to Turner *et al* [3], the circulatory (including diabetes) HR has a value of 1.03 (95% CI: 1.01–1.05), and the respiratory HR has a value of 1.12 (95% CI: 1.08–1.12).

ΔO_g is the difference between the GEOS-Chem simulated and bias-corrected annual average MDA8 ozone concentration and an LCC (low-concentration cutoff). Below the LCC, ozone is assumed to have no effect on mortality. We use choose an LCC value of 26.7 ppbv in the main analysis [3], following previous studies [1, 2].

A previous study [62] shows that at there is no significant difference in ozone-related health impacts at lower end of observed exposures compared to those at higher exposures. Therefore, we also include health

impact estimation without an exposure threshold, that is, choosing 0 ppbv as the LCC instead. The results are shown in supplementary figure 2. Ozone pollution caused by anthropogenic emissions drops below the LCC decades ago, which leads to a sharp decrease of ozone-related premature deaths, such as the sharp change of mortality impacts of upper middle group with its per capita GDP around $1000 as shown in figure 4(a). Choosing 0 ppbv as the LCC narrows the change in the per-million-people contributions to mortality impact of upper middle group when its per capita GDP is around $1000 as shown in supplementary figure 2. Therefore, not only the number of premature deaths get larger, but also the relationship between regional affluence and its ozone mortality impacts gets strengthened.

For each year, we first calculate the total mortality (M_g) due to annual average MDA8 ozone from all anthropogenic and natural sources (after ozone bias corrected; equation (6). We then calculate the number of deaths contributed by each income group by multiplying M_g by the fraction of ozone contributed by that group. Equation (9) provides an example for the high-income group. Mortality contributions of other groups are obtained similarly. Such a direct proportion approach has been used in many previous studies [34, 35, 63, 64]

$$O_g = \text{HIGH}_g + \text{UPPER}_g + \text{LOWER}_g + \text{LOW}_g + \text{NATURE}_g \qquad (8)$$

$$M_g^{\text{HIGH}} = \frac{\text{HIGH}_g}{O_g} \times M_g. \qquad (9)$$

Supplementary figure 8 compares our global total mortality results to other studies. The spread in mortality outcomes reflects the large uncertainty in the current knowledge of the ozone mortality impact. Our results in 2010 are close to the recent study by Shindell *et al* [2] (with ozone bias corrected and with Turner *et al* [3] exposure-response function) on a global total basis.

2.5. Decomposition of changes in ozone-related mortality

Following our previous study [34], historical changes in anthropogenic ozone-related mortality is decomposed into three factors, including baseline mortality rate (*b*), ozone-related term ($T = 1 - e^{-\beta \Delta O}$) and exposed population (*P*), according to the calculation formula in section 2.4.

The change in anthropogenic ozone-related mortality between two simulation years (ΔM) could be expressed as:

$$\Delta M = \Delta b \times T \times P + b \times \Delta T \times P + b \times T \times \Delta P. \qquad (10)$$

Contributions of one factor with the rest two kept constant are denoted by three terms on the right-hand

side. There are six possible decompositions of these three terms, and the averaged decomposition results is used in the main text. See more detailed information in our previous study [34].

2.6. Uncertainty and limitation

This study is subject to uncertainties from a few sources. First, the historical CEDS [37, 49] and MEIC [20, 38–40] inventories used here contain errors ranging from 10% to 170% depending on the pollutant and region, which is further discussed in the limitation discussion below. For our ozone simulations and mortality impact estimates, there errors are embedded in the derivation of the GEOS-Chem model error ($\sigma 1$).

Second, we use the bias between model simulation and measurements to represent the error of GEOS-Chem, following previous studies [34, 63, 64]. Supplementary table 2 shows the mean relative model bias after bias adjustment over mainland China, US, Europe, Canada and globe (combining the four regions together). We use the relative bias over Europe (-14.1%, the worst case) to represent the overall model error. The error is referred to as $\sigma 1$ (one standard deviation).

Third, the ozone exposure-response model by Turner *et al* [3] is subject to errors in linking pollution exposure, specific diseases and premature mortality. We further discuss this as one limitation below. As shown in section 2.4, we use the 95% CI of the HR for respiratory and circulatory diseases to characterize errors in the exposure-response model. The overall error is about 30% and referred to as $\sigma 2$ (one standard deviation).

The overall uncertainty in the historical premature mortality calculation is estimated as the sum in quadrature of $\sigma 1$ and $\sigma 2$. The majority of these error terms do not change with time, thus the temporal changes (in a relative sense) in mortality impacts are less affected by these errors.

Besides the uncertainty sources mentioned before, this study is subjected to several limitations. First, the anthropogenic emission inventories employed in this study tend to contain larger uncertainties in the early years and over some less affluent regions. Therefore, we use other two widely used global anthropogenic emission inventories to explore the linkage between regional affluence level and its ozone precursors' emissions. As shown in supplementary figure 9, the patterns are similar to those in figures 3(c) and (d).

Second, simulated ozone concentrations are all obtained using GEOS-Chem. Although we have employed global surface ozone observations and long-term background ozone observations to validate and adjust the simulated results, further muti-model analyses would be helpful to estimate the intrinsic biases embedded in GEOS-Chem. Although we conduct consistent quality control processes to
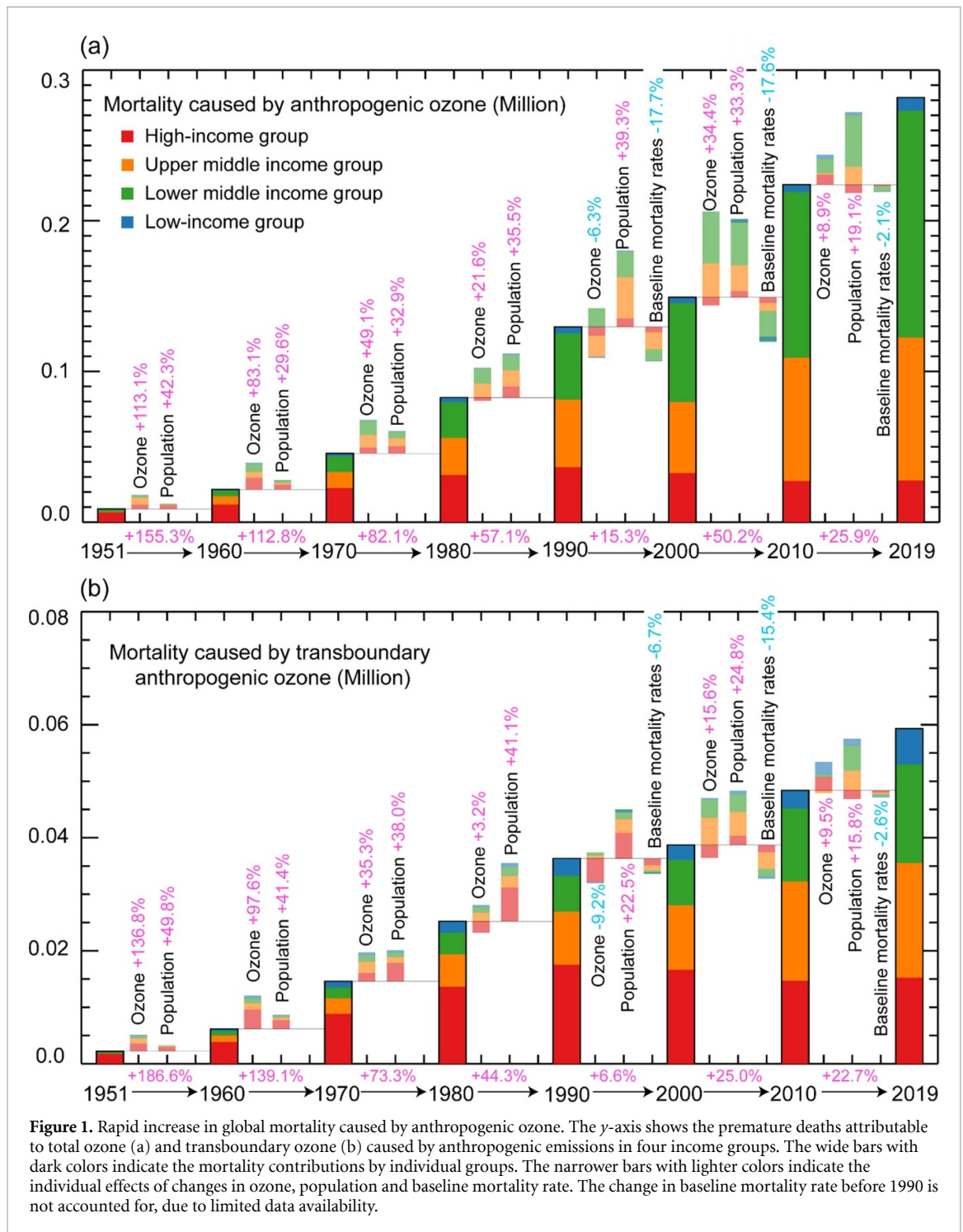
all raw observation datasets in this study, the monitoring networks over different regions have different internal quality control standards and internal procedures [65, 66]. Besides, the surface ozone observations are lacking over less affluent regions [66] (such as rural areas, and globally such as Africa), which could potentially introduce classification error when quantifying ozone exposures [67]. Therefore, we call for improvement in observation metadata reporting, more consistent monitoring procedures in global monitoring networks and more studies focusing on observations and emission datasets over less affluent regions in future to better quantify the uncertainty.

Third, the application of ozone health model is subjected to errors in the internal validity and the generalizability of the health model [67–69]. A full evaluation of this error is technically prohibitive [67]. Following previous studies [1, 2, 34], we estimate the uncertainty ranges, and further conduct sensitivity tests to better address its limitation. Besides the ozone health model from Turner *et al* [3], we also employ another risk function from Jerrett *et al* [60] to estimate the ozone-related premature deaths with similar results to a previous study [1] (supplementary figure 8). We chose 0 ppbv as LCC instead of 26.7 ppbv in another test, which leads to a large number of ozone-related premature deaths and a strengthened relationship between regional affluence and its contribution to mortality caused by transboundary ozone (supplementary figure 2). The baseline mortality rates, as the input datasets, are fixed at 1990 for earlier years, due to data limitation. To test this corresponding effect, we employ linear-extrapolated country-based baseline mortality rates to earlier years and find slightly different mortality results (supplementary figure 3). Further ozone-related cohort studies based on various races, age groups and other socio-economic conditions in future will help to reveal more detailed in transboundary ozone related mortality.

3. Results and discussion

3.1. Aggravating ozone health impact

Figure 1(a) shows the changes in global total premature mortality associated with anthropogenic ozone between about every decade from 1951 to 2019; detailed results for every five years are shown in supplementary figure 10(a). The anthropogenic mortality grows significantly from 8.3 [95% CI: 4.1–12.5] thousand in 1951–129.2 [95% CI: 58.4–199.9] thousand in 1990 and to as large as 281.4 [95% CI: 124.0–438.8] thousand in 2019. Between 1951 and 2019, the global annual mortality attributable to anthropogenic ozone grows by a factor of 34. The premature mortality caused by natural sources, which in 2019 is about 688.6 [95% CI: 303.4–1073.9] thousand and

Figure 1. Rapid increase in global mortality caused by anthropogenic ozone. The *y*-axis shows the premature deaths attributable to total ozone (a) and transboundary ozone (b) caused by anthropogenic emissions in four income groups. The wide bars with dark colors indicate the mortality contributions by individual groups. The narrower bars with lighter colors indicate the individual effects of changes in ozone, population and baseline mortality rate. The change in baseline mortality rate before 1990 is not accounted for, due to limited data availability.

contribute about 71% of the total ozone-related mortality, is not elaborated further in this study.

To better understand the drivers of the increase in anthropogenic ozone mortality impact, we attribute the mortality growth to three factors using a decomposition analysis (section 2.5). The three driving factors considered are ozone concentration, population, and baseline mortality rate. Globally, the baseline mortality rate declines continuously as a result of improved medical and living conditions, based on available data since 1990. However, the increasing ozone concentration and population overcompensate

for the beneficial effect of declining baseline mortality rate and enhance the anthropogenic ozone health burden. The worsening ozone exposure alone causes a 16-fold increase in the total mortality increase from 1951 to 2019, and the population change causes a 24-fold increase over the same period.

The mortality contribution by ozone from each of the four groups has changed substantially over the years. The high-income group contributes as much as 77% of the global total premature mortality in 1951. In absolute terms, ozone from the high-income group leads to 6.4 [95% CI: 2.7–10.1] thousand deaths in

1951, 31.3 [95% CI: 13.1–49.4] thousand in 1980, and 36.4 [95% CI: 15.5–57.4] thousand in 1990. From 1980 to 1990, the ozone concentration contributed by the high-income group declines with its decreasing precursor emissions, but this effect is offset by the growth in global population exposed to ozone pollution originating from the high-income group. Although the mortality caused by the high-income group declines from 1990 and 2010, there is slight growth (by about 1%) from 2010 to 2019. This resumption of mortality growth is primarily because of worsened ozone pollution originating from Europe through the nonlinear chemistry driven by its declining NO_x emissions (supplementary figure 4(a)). The recent worsening European ozone pollution is also found by previous studies based on surface measurements [56, 70–72]. The complex effects of emissions on ozone concentrations and associated mortality highlight the challenges to mitigate ozone pollution.

For the other three groups, their impacts on global ozone mortality have continued to increase since 1951, as a result of general increases in attributable ozone concentration (due to increasing emissions, supplementary figure 4) and population overcompensating the effect of declining baseline mortality rates. As an exception, the decreases in ozone exposure caused by the upper middle and lower middle income groups between 1990 and 2000 are due to significant drop in emissions in many countries [37, 49] which used to be parts of the Soviet Union. By 2019, the premature deaths caused by the upper middle, lower middle and low-income groups reach 94.9 [95% CI: 38.2–151.7] thousand, 150.4 [95% CI: 70.2–230.6] thousand and 8.4 [95% CI: 4.0–12.9] thousand, respectively. In other words, by 2019 the lower middle group becomes the top contributor to annual global premature mortality (53%), followed by the upper middle (34%), high-income (10%) and low-income group (3%).

3.2. Substantial mortality caused by transboundary anthropogenic ozone

Figure 1(b) shows inter-decadal changes in annual premature deaths attributable to transboundary anthropogenic ozone (caused by four source groups but occurring outside their territories) and contributions from the three driving factors (ozone, population and baseline mortality rate) from 1951 to 2019. Results for every five years are shown in supplementary figure 10(b). The mortality attributable to transboundary anthropogenic ozone increases by about 27 times from 2.1 [95% CI: 1.1–3.2] thousand in 1951 to 59 [95% CI: 30–89] thousand in 2019. The worsening ozone pollution alone leads to a 10-fold increase, the rising population causes a 21-fold increase, whereas the declining baseline mortality rate slightly offsets these increases. Between 1951 and
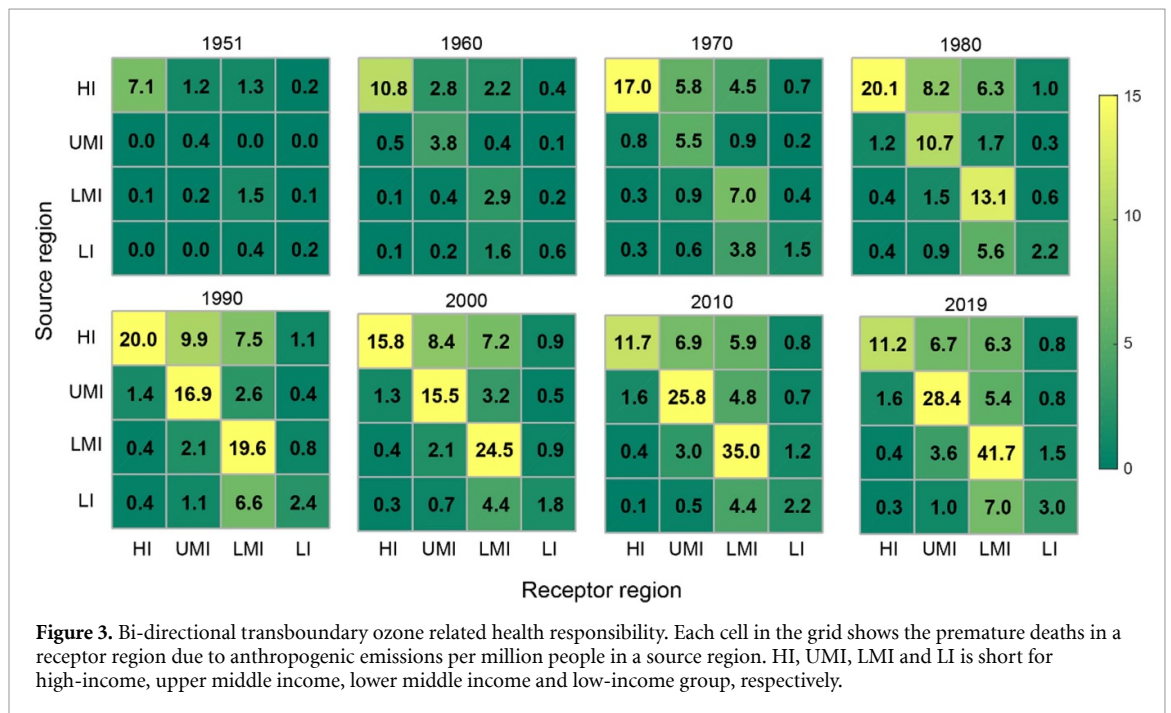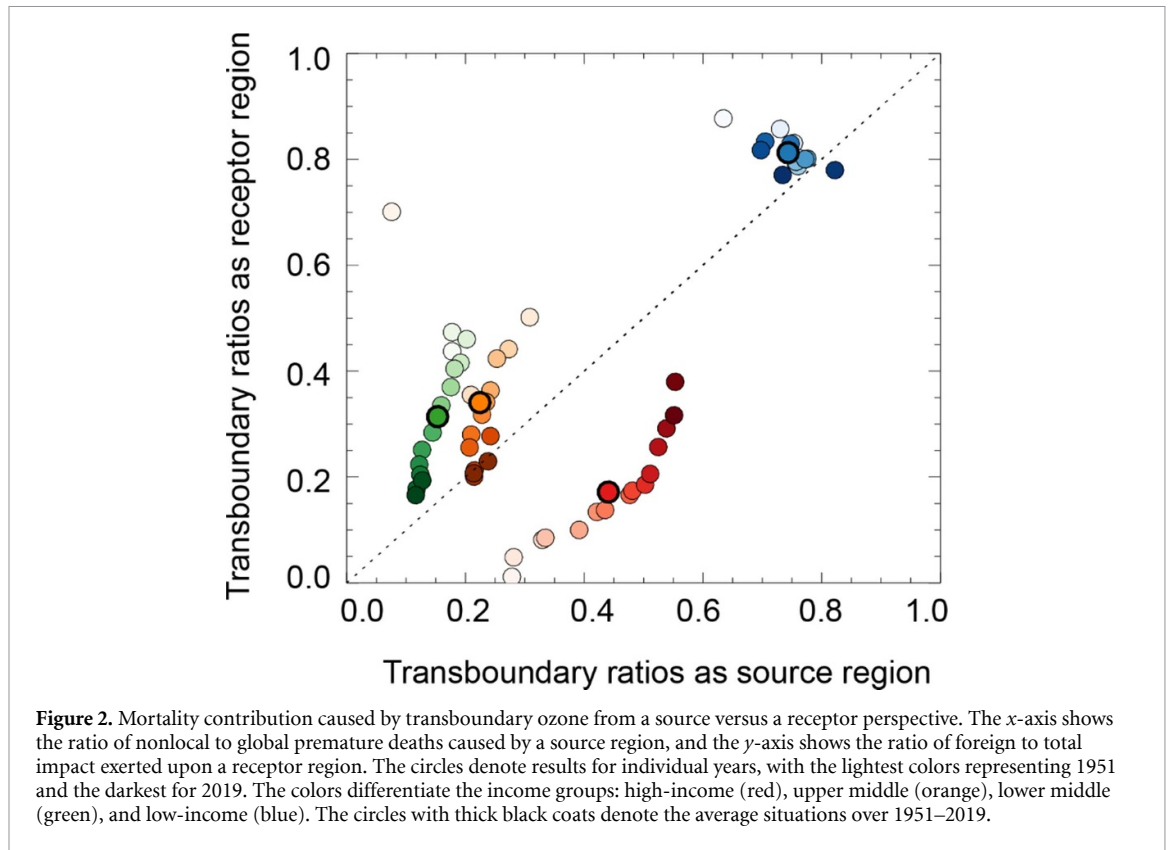
2019, on average, premature deaths caused by transboundary anthropogenic ozone account for about 27% of annual global anthropogenic ozone related deaths.

Ozone originating from the high-income group contributes as much as 84% of annual global mortality caused by transboundary anthropogenic ozone in 1951 and more than 50% before 1990. In absolute terms, the annual contribution of high-income group peaks in 1990 with 17.5 [95% CI: 9.0–26] thousand deaths. The contributions from other three groups increase continuously from 1951 to 2019. In recent decades, the percent contributions of high-income and low-income groups to mortality caused by transboundary ozone are larger than their percentage contributions to total (local + transboundary) mortality (figure 1(b) versus 1a). In 2019, the high-income group contributes about 25.7% of deaths caused by transboundary ozone (figure 1(b)) but only 10% of total ozone related deaths (figure 1(a)), and the respective numbers for the low-income group are 10.5% and 3%. The contributions of upper middle and lower middle groups are about 34.4% and 29.5% in 2019, lower than their contributions to total deaths.

Figure 2 compares the transboundary impact caused by and exerted upon each group, by contrasting the ratio of deaths outside a region's territory and global deaths caused by that region (*x*-axis, as a source) against the ratio of deaths in a region caused by foreign pollution to that region's total deaths (*y*-axis, as receptor). The fractional transboundary impacts both caused by and exerted upon the high-income group are increasing over the past decades to reach 0.6 and 0.3 in 2019, with the former (as a source) always greater than the latter (as a receptor). The fractional transboundary impacts caused by and exerted upon the upper middle and lower middle groups decline with time, as a result of their growing local fractional contributions. The fractional impacts for the low-income group remain at high values of 0.6–0.9 throughout the years, reflecting stable, strong tie of its ozone problem with other groups.

Figure 3 shows the transboundary ozone related mortality inter-impacts between the four groups, in terms of the impact of every million people in a source region, for every decade. Supplementary figure 11 presents detailed information for all simulation years. In 1951, emissions of every one million people in the high-income group cause 1.2 [95% CI: 0.5–1.9] premature deaths in the upper middle group and 1.3 [95% CI: 0.6–2.0] in the lower middle group. The respective effects change to 9.9 [95% CI: 4.0–15.8] and 7.5 [95% CI: 3.6–11.5] in 1990 and 6.7 [95% CI: 2.5–10.8] and 6.3 [95% CI: 2.8–9.8] in 2019. These values are comparable to (over 1960–1975) or even higher than (in 1951) the self-impacts of upper middle and lower middle groups.

Figure 3 also shows that the mortality impacts attributable to transboundary ozone caused by every

Figure 2. Mortality contribution caused by transboundary ozone from a source versus a receptor perspective. The *x*-axis shows the ratio of nonlocal to global premature deaths caused by a source region, and the *y*-axis shows the ratio of foreign to total impact exerted upon a receptor region. The circles denote results for individual years, with the lightest colors representing 1951 and the darkest for 2019. The colors differentiate the income groups: high-income (red), upper middle (orange), lower middle (green), and low-income (blue). The circles with thick black coats denote the average situations over 1951–2019.

Figure 3. Bi-directional transboundary ozone related health responsibility. Each cell in the grid shows the premature deaths in a receptor region due to anthropogenic emissions per million people in a source region. HI, UMI, LMI and LI is short for high-income, upper middle income, lower middle income and low-income group, respectively.
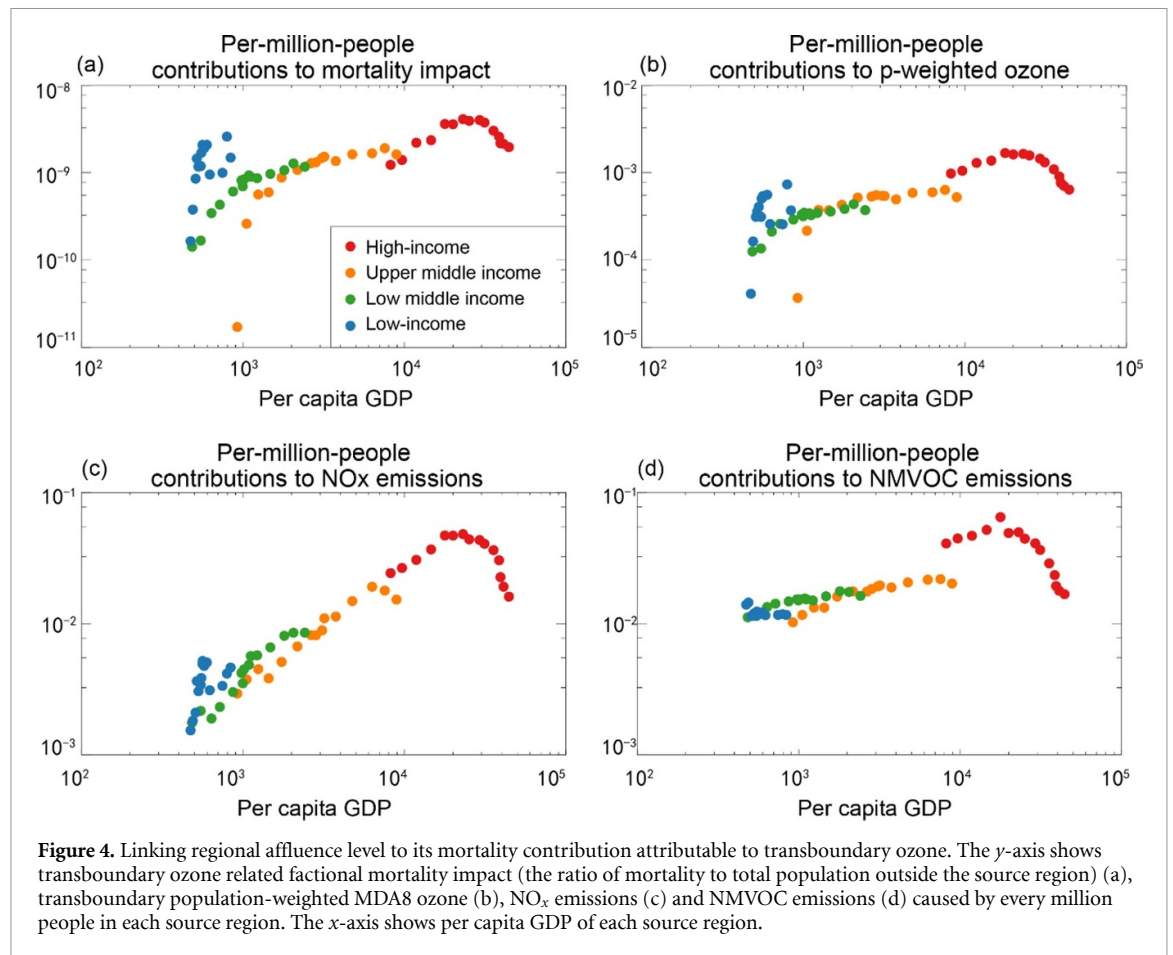
million people of the other three groups reach their maximum values in 2019. However, in this year the impacts of upper middle and lower middle groups on the high-income group are still smaller than the reciprocal impacts (1.6 [95% CI: 0.7–2.5] versus 6.7 [95% CI: 2.5–10.8], and 0.4 [95% CI: 0.2–0.7] versus 6.3 [95% CI: 2.8–9.8]). This is due to the regional differences in population exposed to ozone and in baseline mortality rate. The same phenomenon exists between the upper middle and the lower middle groups.

3.3. Linkage between mortality attributable to transboundary ozone and affluence
Figure 4 links the transboundary impact by every million people in a given group (as a source region) to its affluence level (i.e. per capita GDP), by putting together data in all groups and years. This allows

Figure 4. Linking regional affluence level to its mortality contribution attributable to transboundary ozone. The *y*-axis shows transboundary ozone related factional mortality impact (the ratio of mortality to total population outside the source region) (a), transboundary population-weighted MDA8 ozone (b), NO_x emissions (c) and NMVOC emissions (d) caused by every million people in each source region. The *x*-axis shows per capita GDP of each source region.

to evaluate the evolution of regional transboundary ozone impact in association with affluence from a macroscopic, socioeconomic perspective. We examine the per-million-people contributions of each source region to its transboundary ozone related fractional mortality impact (FMI, the ratio of mortality number to total population; figure 4(a)), to transboundary population-weighted MDA8 ozone (figure 4(b)), and to its own NO_x (figure 4(c)) and NMVOC (figure 4(d)) emissions. Analysis of transboundary FMI caused by every million people in each source region removes the influence of historical population growth. Results for local FMI are shown in supplementary figure 12 for comparison.

For the high-income group, a clear inverted U-shaped relationship exists between its affluence level and per-million-people transboundary FMI (figure 4(a)). The transboundary FMI increases with affluence until a turning point, after which the transboundary FMI decreases substantially with further increasing affluence. The per capita GDP at the turning point is about 23 000 USD. Similar inverted U-shaped patterns are evident for this group in per-million-people contributions to transboundary ozone, NO_x emissions and NMVOC emissions (figures 4(b)–(d)).

For the upper middle group, its per-million-people NO_x emissions peak at an affluence level of

about 6300 USD, which is much lower than the turning point of high-income group. The lower turning point is partly due to emission control measurements in China [20, 37, 49], which belongs to this group. Prior to this turning point, the upper middle group follows the growth pattern of per-million-people NO_x emissions of the high-income group. Per-million-people NMVOC emissions of the upper middle group deviate from the path of high-income group and start to decline at an affluence level around 7500 USD.

For the upper middle group, its per-million-people transboundary FMI is very small when the affluence level is below 1000 USD, but grows substantially with affluence to quickly match the path of high-income group until a turning point similar to those for precursor emissions. The small mortality impact at low-affluence situations is because ozone concentrations are below the LCC (26.7 ppbv) in many downwind regions of the upper middle group. There is emerging evidence that the health impact of ozone may not have such an exposure threshold [62]. Removing this threshold would substantially increase the mortality impact at low-affluence situations (supplementary figure 2).

Per-million-people NO_x and NMVOC emissions and transboundary ozone impact of the lower middle group have followed similar paths as the upper middle group, albeit with some differences at low affluence

situations around 1000 USD. For the per-million-people transboundary FMI, the gap between the paths of lower middle and upper middle groups narrows down along with the increasing affluence level.

Among the four source regions, the low-income group has undergone the weakest growth in affluence in both absolute and relative terms. For this group, there is substantial scattering in its per-million-people emissions, transboundary ozone and mortality impact. The relatively small changes in affluence render an affluence-pollution relationship more difficult to be established.

4. Conclusion

This study shows considerable transboundary ozone related premature mortality over the course of 1951–2019 and its evolution with regional affluence. Bi-directional transboundary pollution between less and more affluent regions are substantial. The high-income group has undergone an inverted U-shaped pattern between its affluence and its mortality impact caused by transboundary ozone, after removing the effect of historical population growth in both source and receptor regions. The upper middle group has experienced a turning point at a lower affluence level, whereas turning points are not obvious in the lower middle and low-income groups.

As less affluent countries try to achieve sustained economic growth, they continue to suffer from increasing pollutant emissions in general. Starting at a low-affluence turning point to invert this emission trend will have local and nonlocal health benefits via atmospheric transport. This task is possible, because the scientific knowledge and financial and technical capabilities for ozone control nowadays are much better than decades ago [73]; the turning point of the upper middle group at an affluence level much lower than the high-income group is strong evidence. Although the short-term economic costs of pollution mitigation can be substantial for less affluent regions, such burden can be compensated by its health benefits [2, 5, 74]. Stringent mitigation policies may also provide new opportunities for technological innovation [19, 75, 76], efficiency improvement [77, 78], and labor demand enhancement [79, 80]. Measures to cut pollutant emissions often reduce carbon dioxide simultaneously with substantial co-benefits for climate change mitigation.

Besides domestic actions by less affluent countries to reduce emissions, international financial and technological aids from more affluent countries would lead to a win-win health outcome. This is important especially given that large fractions of present emissions in less affluent countries are associated with export of goods to supply consumption worldwide [35, 36] in a globalized economy. To this end, our study offers a socioeconomic insight into historical inter-regional pollution linkage to facilitate concerted mitigation action.

Data availability statement

Acknowledgments

Author contributions

Jintai Lin and Lulu Chen conceived and designed the research. Lulu Chen performed the research. Ruijing Ni, Hongjian Weng, Yingying Yan and Hao Kong contributed to model simulations. Lulu Chen and Jintain Lin led the analysis with inputs from Randall Marin, Mingxi Du, Yuanhong Zhao and Jingxu Wang. Lulu Chen and Jintai Lin wrote the paper and all authors commented on the writing.

Conflict of interest

The authors declare that they have no conflict of interest.

ORCID iDs

Lulu Chen ⬤ https://orcid.org/0000-0002-8929-3414
Jintai Lin ⬤ https://orcid.org/0000-0002-2362-2940
Mingxi Du ⬤ https://orcid.org/0000-0002-6831-4255
Mengyao Liu ⬤ https://orcid.org/0000-0001-7609-067X
Jingxu Wang ⬤ https://orcid.org/0000-0002-5642-9880
Hongjian Weng ⬤ https://orcid.org/0000-0003-1886-9452

References

[1] Malley C S, Henze D K, Kuylenstierna J C I, Vallack H W, Davila Y, Anenberg S C, Turner M C and Ashmore M R 2017 Updated global estimates of respiratory mortality in adults ⩾ 30 Years of age attributable to long-term ozone exposure *Environ. Health Perspect.* **125** 087021

[2] Shindell D, Faluvegi G, Seltzer K and Shindell C 2018 Quantified, localized health benefits of accelerated carbon dioxide emissions reductions *Nat. Clim. Change* **8** 291–5

[3] Turner M C *et al* 2016 Long-term ozone exposure and mortality in a large prospective study *Am. J. Respir. Crit. Care Med.* **193** 1134–42

[4] Malley C S *et al* 2021 Integrated assessment of global climate, air pollution, and dietary, malnutrition and obesity health impacts of food production and consumption between 2014 and 2018 *Environ. Res. Commun.* **3** 075001

[5] Shindell D *et al* 2021 Temporal and spatial distribution of health, labor, and crop benefits of climate change mitigation in the United States *Proc. Natl Acad. Sci.* **118** e2104061118

[6] X-b L and Fan G 2022 Interannual variations, sources, and health impacts of the springtime ozone in Shanghai *Environ. Pollut.* **306** 119458

[7] Wang Y, Xie M, Wu Y, Zhang X, Wang M, Zhang Y and Xie Y 2022 Ozone-related Co-benefits of China's climate mitigation policy *Resour. Conserv. Recycl.* **182** 106288

[8] Sheng L, Qin M, Li L, Wang C, Gong K, Liu T, Li J and Hu J 2022 Impacts of emissions along the lower Yangtze River on air quality and public health in the Yangtze River delta, China *Atmos. Pollut. Res.* **13** 101420

[9] Malashock D A, Delang M N, Becker J S, Serre M L, West J J, Chang K-L, Cooper O R and Anenberg S C 2022 Estimates of ozone concentrations and attributable mortality in urban, peri-urban and rural areas worldwide in 2019 *Environ. Res. Lett.* **17** 054023

[10] Zhang X, Cheng C and Zhao H 2022 A health impact and economic loss assessment of O_3 and PM2.5 exposure in China From 2015 to 2020 *GeoHealth* **6**

[11] Liang C K *et al* 2018 HTAP2 multi-model estimates of premature human mortality due to intercontinental transport of air pollution and emission sectors *Atmos. Chem. Phys.* **18** 10497–520

[12] Anenberg S C *et al* 2009 Intercontinental impacts of ozone pollution on human mortality *Environ. Sci. Technol.* **43** 6482–7

[13] Dedoussi I C, Eastham S D, Monier E and Barrett S R H 2020 Premature mortality related to United States cross-state air pollution *Nature* **578** 261–5

[14] Ni R J, Lin J T, Yan Y Y and Lin W L 2018 Foreign and domestic contributions to springtime ozone over China *Atmos. Chem. Phys.* **18** 11447–69

[15] Howarth N, Galeotti M, Lanza A and Dubey K 2017 Economic development and energy consumption in the GCC: an international sectoral analysis *Energy Transit.* **1** 1–19

[16] Arto I, Capellan-Perez I, Lago R, Bueno G and Bermejo R 2016 The energy requirements of a developed world *Energy Sustain. Dev.* **33** 1–13

[17] Xu B, Zhong R, Liu D and Liu Y 2021 Investigating the impact of energy consumption and nitrogen fertilizer on NO_x emissions in China based on the environmental Kuznets curve *Environ. Dev. Sustain.* **23** 17590–605

[18] Feng T W, Sun L Y and Zhang Y 2009 The relationship between energy consumption structure, economic structure and energy intensity in China *Energy Policy* **37** 5475–83

[19] Liu X *et al* 2019 Updated hourly emissions factors for Chinese power plants showing the impact of widespread ultralow emissions technology deployment *Environ. Sci. Technol.* **53** 2570–8

[20] Zheng B *et al* 2018 Trends in China's anthropogenic emissions since 2010 as the consequence of clean air actions *Atmos. Chem. Phys.* **18** 14095–111

[21] Ru M Y, Shindell D T, Seltzer K M, Tao S and Zhong Q R 2018 The long-term relationship between emissions and economic growth for SO_2, CO_2, and BC *Environ. Res. Lett.* **13** 124021

[22] Huang T, Zhu X, Zhong Q, Yun X, Meng W, Li B, Ma J, Zeng E Y and Tao S 2017 Spatial and temporal trends in global emissions of nitrogen oxides from 1960 to 2014 *Environ. Sci. Technol.* **51** 7992–8000

[23] Selden T M and Song D 1994 Environmental quality and development: is there a kuznets curve for air pollution emissions? *J. Environ. Econ. Manage.* **27** 147–62

[24] Georgiev E and Mihaylov E 2015 Economic growth and the environment: reassessing the environmental kuznets curve for air pollution emissions in OECD countries *Lett. Spatial Resour. Sci.* **8** 29–47

[25] Cohan D S, Hakami A, Hu Y and Russell A G 2005 Nonlinear response of ozone to emissions: source apportionment and sensitivity analysis *Environ. Sci. Technol.* **39** 6739–48

[26] Lin X, Trainer M and Liu S C 1988 On the nonlinearity of the tropospheric ozone production *J. Geophys. Res.* **93** 15879

[27] Seinfeld J H and Pandis S N 2016 *Atmospheric Chemistry and Physics: From Air Pollution to Climate Change* Third ed (New York Wiley)

[28] McKitrick R and Wood J 2017 An examination of the relationship between air quality and income in Canada *Can. J. Agric. Econ.* **65** 69–92

[29] Shen F, Zhang L, Jiang L, Tang M, Gai X, Chen M and Ge X 2020 Temporal variations of six ambient criteria air pollutants from 2015 to 2018, their spatial distributions, health risks and relationships with socioeconomic factors during 2018 in China *Environ. Int.* **137** 105556

[30] Plassmann F and Khanna N 2006 Household income and pollution *J. Environ. Dev.* **15** 22–41

[31] Zhang L, Jacob D J, Kopacz M, Henze D K, Singh K and Jaffe D A 2009 Intercontinental source attribution of ozone pollution at western U.S. sites using an adjoint method *Geophys. Res. Lett.* **36**

[32] Wu S, Duncan B N, Jacob D J, Fiore A M and Wild O 2009 Chemical nonlinearities in relating intercontinental ozone pollution to anthropogenic emissions *Geophys. Res. Lett.* **36**

[33] United Nations Departments of Economic and Social Affairs *World Economic Situation and Prospects* 2018 (New York: United Nations) (https://doi.org/10.18356/02486bd4-en)

[34] Chen L *et al* 2021 Inequality in historical transboundary anthropogenic PM2.5 health impacts *Sci. Bull.* **67** 437–44

[35] Zhang Q *et al* 2017 Transboundary health impacts of transported global air pollution and international trade *Nature* **543** 705–9

[36] Lin J, Pan D, Davis S J, Zhang Q, He K, Wang C, Streets D G, Wuebbles D J and Guan D 2014 China's international trade and air pollution in the United States *Proc. Natl Acad. Sci. USA* **111** 1736–41

[37] Hoesly R M *et al* 2018 Historical (1750–2014) anthropogenic emissions of reactive gases and aerosols from the community emissions data system (CEDS) *Geosci. Model Dev.* **11** 369–408

[38] Li M *et al* 2017 Anthropogenic emission inventories in China: a review *Natl Sci. Rev.* **4** 834–66

[39] Department of Earth System Science Tsinghua University *Multi-resolution emission inventory for China* (available at: www.meicmodel.org) (Accessed 18 November 2018)

[40] Geng G N, Zhang Q, Martin R V, Lin J T, Huo H, Zheng B, Wang S and He K 2017 Impact of spatial proxies on the representation of bottom-up emission inventories: a satellite-based analysis *Atmos. Chem. Phys.* **17** 4131–45

[41] GEOS-Chem v11-01 2017 *GEOS-Chem overview* (available at: http://wiki.seas.harvard.edu/geos-chem/index.php/Main_Page) (Accessed 1 February 2017)

[42] Global Burden of Disease Collaborative Network 2020 Global burden of disease study 2019 (GBD 2019) results (Seattle: Institute for Health Metrics and Evaluation (IHME)) (available at: http://ghdx.healthdata.org/gbd-results-tool)

[43] Butt E W, Turnock S T, Rigby R, Reddington C L, Yoshioka M, Johnson J S, Regayre L A, Pringle K J, Mann G W and Spracklen D V 2017 Global and regional trends in particulate air pollution and attributable health burden over the past 50 years *Environ. Res. Lett.* **12** 104017

[44] World Bank Group *World Bank Open Data* (available at: https://data.worldbank.org/) (Accessed 9 August 2020)

[45] Lin J T, Liu Z, Zhang Q, Liu H, Mao J and Zhuang G 2012 Modeling uncertainties for tropospheric nitrogen dioxide

columns affecting satellite-based inverse modeling of nitrogen oxides emissions *Atmos. Chem. Phys.* **12** 12255–75

[46] Lin J T and McElroy M B 2010 Impacts of boundary layer mixing on pollutant vertical profiles in the lower troposphere: implications to satellite remote sensing *Atmos. Environ.* **44** 1726–39

[47] Moorthi S and Suarez M J 1992 Relaxed Arakawa-Schubert—a parameterization of moist convection for general-circulation models *Mon. Weather Rev.* **120** 978–1002

[48] McLinden C A, Olsen S C, Hannegan B, Wild O, Prather M J and Sundet J 2000 Stratospheric ozone in 3D models: a simple chemistry and the cross-tropopause flux *J. Geophys. Res.* **105** 14653–65

[49] McDuffie E E, Smith S J, O'Rourke P, Tibrewal K, Venkataraman C, Marais E A, Zheng B, Crippa M, Brauer M and Martin R V 2020 A global anthropogenic emission inventory of atmospheric pollutants from sector- and fuel-specific sources (1970–2017): an application of the community emissions data system (CEDS) *Earth Syst. Sci. Data* **12** 3413–42

[50] United States Environmental Protection Agency *Air Data: Air Quality Data Collected at Outdoor Monitors Across the US* (available at: www.epa.gov/outdoor-air-quality-data) (Accessed 3 March 2018)

[51] Environment and Climate Change Canada *National air pollution surveillance (NAPS) program* (available at: http://maps-cartes.ec.gc.ca/rnspa-naps/data.aspx?lang=en) (Accessed 3 March 2018)

[52] EMEP/CEIP 2014 Present state of emission data (available at: www.ceip.at/ms/ceip_home1/ceip_home/webdab_emepdatabase/reported_emissiondata) (Accessed 28 September 2015)

[53] China Environmental Monitoring Station 2010 *Real-time data* (available at: www.cnemc.cn/sssj/) (Accessed 5 November 2018)

[54] Lu X, Hong J Y, Zhang L, Cooper O R, Schultz M G, Xu X B, Wang T, Gao M, Zhao Y and Zhang Y 2018 Severe surface ozone pollution in china: a global perspective *Environ. Sci. Technol. Lett.* **5** 487–94

[55] Yan Y Y, Lin J T and He C L 2018 Ozone trends over the United States at different times of day *Atmos. Chem. Phys.* **18** 1185–202

[56] Yan Y Y, Lin J T, Pozzer A, Kong S F and Lelieveld J 2019 Trend reversal from high-to-low and from rural-to-urban ozone concentrations over Europe *Atmos. Environ.* **213** 25–36

[57] Global Burden of Disease Collaborative Network 2017 Global burden of disease study 2016 (GBD 2016) results (Seattle: Institute for Health Metrics and Evaluation (IHME)) (available at: http://ghdx.healthdata.org/gbd-results-too)

[58] United Nations, Department of Economic and Social Affairs 2019 *Population Division* (available at: https://population.un.org/wpp/) (Accessed 28 December 2019)

[59] Schultz M G *et al* 2017 Tropospheric Ozone Assessment Report: Database and Metrics Data of Global Surface Ozone Observations *Elementa Sci. Anthrop.* **5** 58

[60] Jerrett M, Burnett R T, Pope C A 3rd, Ito K, Thurston G, Krewski D, Shi Y, Calle E and Thun M 2009 Long-term ozone exposure and mortality *New Engl. J. Med.* **360** 1085–95

[61] Nasari M M *et al* 2016 A class of non-linear exposure-response models suitable for health impact assessment applicable to large cohort studies of ambient air pollution *Air Qual. Atmos. Health* **9** 961–72

[62] Di Q, Wang Y, Zanobetti A, Wang Y, Koutrakis P, Choirat C, Dominici F and Schwartz J D 2017 Air pollution and mortality in the medicare population *New Engl. J. Med.* **376** 2513–22

[63] Lin J *et al* 2019 Carbon and health implications of trade restrictions *Nat. Commun.* **10** 4947

[64] Du M X *et al* 2020 Winners and losers of the Sino-US trade war from economic and environmental perspectives *Environ. Res. Lett.* **15** 094032

[65] Schultz M G *et al* 2017 Tropospheric ozone assessment report: database and metrics data of global surface ozone observations *Elem.-Sci. Anthrop.* **5**

[66] Sofen E D *et al* 2016 Gridded global surface ozone metrics for atmospheric chemistry model evaluation *Earth Syst. Sci. Data* **8** 41–59

[67] Rothman K J and Greenland S 2005 Validity and generalizability in epidemiologic studies *Encyclopedia of Biostatistics* (New York: Wiley) (https://doi.org/10.1002/0470011815.b2a03129)

[68] Ange B A, Symons J M, Schwab M, Howell E and Geyh A 2004 Generalizability in epidemiology: an investigation within the context of heart failure studies *Ann. Epidemiol.* **14** 600–1

[69] Fann N, Bell M L, Walker K and Hubbell B 2011 Improving the linkages between air pollution epidemiology and quantitative risk assessment *Environ. Health Perspect.* **119** 1671–5

[70] Finch D P and Palmer P I 2020 Increasing ambient surface ozone levels over the UK accompanied by fewer extreme events *Atmos. Environ.* **237** 117627

[71] Sicard P, Agathokleous E, De Marco A, Paoletti E and Calatayud V 2021 Urban population exposure to air pollution in Europe over the last decades *Environ. Sci. Eur.* **33** 1–12

[72] Sicard P, Paoletti E, Agathokleous E, Araminienė V, Proietti C, Coulibaly F and De Marco A 2020 Ozone weekend effect in cities: deep insights for urban air pollution control *Environ. Res.* **191** 110193

[73] Rao S *et al* 2017 Future air pollution in the shared socio-economic pathways *Glob. Environ. Change-Hum. Policy Dimensions* **42** 346–58

[74] Shindell D and Smith C J 2019 Climate and air-quality benefits of a realistic phase-out of fossil fuels *Nature* **573** 408–11

[75] Carraro C and Siniscalco D 1994 Technical innovation and environmental-protection—environmental-policy reconsidered—the role of technological innovation *Eur. Econ. Rev.* **38** 545–54

[76] Taylor M R, Rubin E S and Hounshell D A 2003 Effect of government actions on technological innovation for SO_2 control *Environ. Sci. Technol.* **37** 4527–34

[77] Hasanbeigi A, Morrow W, Masanet E, Sathaye J and Xu T F 2013 Energy efficiency improvement and CO_2 emission reduction opportunities in the cement industry in China *Energy Policy* **57** 287–97

[78] Tong D *et al* 2018 Current emissions and future mitigation pathways of coal-fired power plants in China from 2010 to 2030 *Environ. Sci. Technol.* **52** 12905–14

[79] Conrad K and Loschel A 2005 Recycling of eco-taxes, labor market effects and the true cost of labor—a CGE analysis *J. Appl. Econ.* **8** 259–78

[80] Küster R, Ellersdorfer I R and Fahl U 2007 A CGE-analysis of energy policies considering labor market imperfections and technology specifications *SSRN Electron. J.* (https://doi.org/10.2139/ssrn.96072)